Research Article

Environmental Chemistry and Safety
DOI: 10.26599/ECS.2026.9600005
2026, 2, 9600005

Facile fabrication of covalent organic framework (COF-LZU1) membrane for water recovery from saline oil-in-water emulsion via membrane distillation

Zhihang Liu[1,3], Jun Li[2], Hengyi Zhang[3], Long-Fei Ren[1,3,4*], and Jiahui Shao[1]

[1]Yazhou Bay Institute of Deepsea Science and Technology, Hainan Research Institute, Shanghai Jiao Tong University, Sanya 572025, PR China

[2]School of Chemistry and Chemical Engineering, Shanghai University of Engineering Science, No. 333 Longteng Road, Shanghai 201620, PR China

[3]State Key Laboratory of Green Papermaking and Resource Recycling, School of Environmental Science and Engineering, Shanghai Jiao Tong University, No. 800 Dongchuan Road, Shanghai 200240, PR China

[4]Chongqing Research Institute, Shanghai Jiao Tong University, No. 598 Liangjiang Road, Chongqing 401135, PR China

Abstract: Membrane fouling and wetting are the main challenges for membrane distillation (MD) that constrains its application especially in water recovery from saline oil-in-water emulsion. Herein, a novel covalent organic framework (COF) modified membrane was developed via facile in-situ growth of COF-LZU1 (synthesized by p-phenylenediamine and 1,3,5-benzenetricarboxaldehyde) on electrospun polyvinylidene fluoride (PVDF) substrate (average pore size: 0.80 μm, average porosity: 85.5%). This newly developed membrane exhibited high surface roughness (1.22 μm), suitable porosity (57.3%), well-distributed pore size (0.67 μm) and thin thickness (58.0 μm). In addition, the hydrophilic COF-LZU1 layer (water contact angle 79.9°) and hydrophobic PVDF substrate (water contact angle 140.5°) endowed this Janus-like membrane with high fouling and wetting resistance. As a result, relatively higher water flux and milder conductivity increase were shown on COF-LZU1@PVDF-2 membrane during the treatment for saline oil-in-water emulsion with 0.0-4.0 g L^{-1} *n*-hexadecane and 50-80°C feed temperature. The anti-fouling and anti-wetting mechanisms were also quantitatively investigated by the extended Derjaguin–Landau–Verwey–Overbeek (XDLVO) theory and liquid entry pressure (LEP) value. The relevant findings may pave the way in high performance COF modified membrane development with high water flux and high permeate quality for robust membrane distillation.

Key words: Membrane distillation; saline oil-in-water emulsion; covalent organic framework; membrane fouling.

Citation: Liu Z H, Li J, Zhang H Y, et al. Facile fabrication of covalent organic framework (COF-LZU1) membrane for water recovery from saline oil-in-water emulsion via membrane distillation. *Environmental Chemistry and Safety*, 2026, 2, 9600005. https://doi.org/10.26599/ECS.2026.9600005

1. Introduction

Petrochemical industry is a fundamental industry of China that plays a vitally important role in economic growth and social development[1]. However, the major concern within the petrochemical industry is its enormous freshwater consumption which is inevitably transformed into petrochemical wastewater. It is estimated that about 4.0 billion tons of petrochemical wastewaters are annually discharged in China, which usually contain high amounts of refractory, toxic oils (*e.g. n*-hexadecane) and high salinity (*e.g.* sodium chloride (NaCl))[1,2]. Biological-related process, including activated sludge process, membrane bioreactor, is one of the main approaches for petrochemical wastewater treatment, unfortunately, it is still highly challenging due to biorefractory organic and hypersaline inorganic pollutants[3].

In comparison, membrane distillation (MD) is considered a promising technology for petrochemical wastewater treatment due to its high less-volatile oils rejection, high salinity tolerance, high permeate quality, low operation demand, environmentally-friendliness and cost-effectiveness[4]. As a thermal-driven membrane separation process using microporous hydrophobic membrane, MD could separate water vapor from hot feed side and then condense water vapor to purified distillate at cold permeate side, while the less-volatile oils and salts are completely retained in feed side[5]. Suitable membrane is the guarantee to achieve this selective separation, and membrane development has been the main focus for MD field in recent years[6,7]. Among various candidates, electrospun membrane prepared from fluoropolymers (*e.g.* poly(vinylidene fluoride), PVDF) usually exhibits favorable process-ability, controllable thickness, high porosity, high surface roughness, abundant pore-interconnectivity and sufficient hydrophobicity[8,9], which has been interested increasingly in MD.

In spite of various advantages, the application of common electrospun membrane in wastewater treatment inevitably suffers from membrane fouling especially facing the oil-in-water emulsion. Hydrophobic oil compounds usually show high affinity to the hydrophobic membrane via hydropho-

Correspondence to: Ren L F, longfeiren@sjtu.edu.cn
Received: December 3, 2025; Revised: January 5, 2026; Accepted: January 12, 2026

bic-hydrophobic interaction[10]. Thus, membrane fouling would occur with the oil deposition on membrane surface or in internal pores[11], which dramatically restricts water vapor transport and even significantly compromises permeate quality once membrane is wetted[12]. For example, during the treatment for saline oil-in-water emulsion with 1000 mg L^{-1} lubricating oil and 3.5 wt.% NaCl, the superhydrophobic PVDF membrane modified by silica nanoparticles still severely suffered from membrane fouling, and the water flux rapidly dropped from 25.0 to 0 kg m^{-2} h^{-1} within 150 min[13]. Therefore, there is an urgent need to improve the electrospun membrane with robust anti-fouling and anti-wetting properties in MD against hydrophobic oil compounds.

It is widely accepted that the surface hydrophilic modifications via doping, deposition and grafting are able to reduce tendency toward hydrophobic oil compounds[14]. The hydrophilic layer could induce a hydration shell facing feed side and exhibit oleophobic during MD process. Therefore, the deposition of hydrophobic oil on membrane surface via hydrophobic-hydrophobic interaction would be limited, thus protecting membrane from fouling. Recently, covalent organic frameworks (COFs), as an emerging class of crystalline porous materials, receives growing interests in membrane hydrophilic modification fields due to its unique structures and intrinsic properties[15,16]. COFs is usually constructed from organic building blocks into periodically ordered and extended two- or three-dimensional network structures via covalent bonds[17], which endows COFs with tailorable pores structure, ordered channel structure, high chemical stability and large surface area[18,19]. These attributes enable COF-based membranes to be successfully utilized in water/wastewater treatment, gas separation, organic solvent separation, and pervaporation. For example, *Wang et al.* fabricated a novel nanofiltration membrane by incorporating amine-rich COF material (SNW-1) into the polyamide layer via interfacial polymerization[20]. During nanofiltration, the SNW-1-modified membrane exhibited a 92% increase in water flux compared to the pristine membrane, which was attributed to its improved surface hydrophilicity and enhanced porous structure[20]. In addition, the COF-based membrane exhibits unique potential for MD. *Zhao et al.* developed a novel MD membrane with a hydrophilicity gradient by engineering defects in COF_{DT}, which was covalently linked 2,5-dihydroxy-1,4-benzenedicarboxaldehyde and 1,3,5-tris(4-aminophenyl)-benzene[21]. The incorporation of COF_{DT} on commercial PVDF membrane endowed this membrane with remarkable water flux of 600 kg m^{-2} h^{-1} and capabilities of anti-fouling and anti-wetting during operation[21]. In theory, water evaporation in MD process might be promoted near the nano-confined pore structures of COFs via reducing free energy barrier for vaporization. The straight channels of COFs reduce the water vapor diffusion length and molecule reflection for water permeation flux improvement. The ultra-small pore size of COFs also efficiently prevent the invasion of water, salts and oils as a molecular sieving barrier[22]. These attributes make COFs serve as an ideal material for MD membrane with robust desalination performance and sufficient fouling, wetting resistance. Nevertheless, membrane preparation/modification based on COFs and its application in MD process still has not been paid enough attention.

Therefore, the purpose of present study was to develop a novel COF modified membrane for robust MD desalination performance in dealing with saline oil-in-water emulsion. Herein, 2D COF-LZU1 synthesized by p-phenylenediamine and 1,3,5-benzenetricarboxaldehyde, was used for in-situ growth on electrospun PVDF substrate. Typical pollutants in petrochemical wastewater, *n*-hexadecane and NaCl were selected to prepare the saline oil-in-water emulsion. This newly developed COF-LZU1 modified membrane was used in MD for the first time to deal with saline oil-in-water emulsion. The membrane properties including morphology, roughness, pore size, porosity, functional group, composition and wettability of pristine PVDF membrane and COF-LZU1 modified membranes were characterized for comparison. Desalination performance of these membranes in MD was also evaluated in terms of water flux and permeate conductivity. Furthermore, the anti-fouling and anti-wetting behavior and mechanism before and after COF-LZU1 modification were investigated by extended Derjaguin-Landau-Verwey-Overbeek (XDLVO) theory and liquid entry pressure (LEP) value, respectively.

2. Materials and Methods

2.1. Materials

PVDF (Solef 6020, Mw: 670-700 kDa), dimethylacetamide (DMAc, Aladdin, 99%) and acetone (Sinopharm, ⩾99.5%) were used to prepare the pristine PVDF electrospun nanofibrous membranes. 1,3,5-Benzenetricarboxaldehyde (TFB, Aladdin, 97%), p-phenylenediamine (PDA, Aladdin, 97%), 1,4-dioxane (Aladdin, 99%), acetic acid (Sinopharm, 99.8%) and ethanol (Aladdin, 99.8%) were used for further COF-LZU1 modification. NaCl (Sinopharm, 99.5%) and *n*-hexadecane (Sinopharm, 98%) were used to prepare saline oil-in-water emulsion. Deionized (DI) water, glycerol (Aladdin, 99%), diiodomethane (Aladdin, 98%) were used in surface tension measurement. All working solutions were prepared using the received chemicals without further treatment and the ultrapure water produced by Millipore Milli-Q system, unless otherwise stated.

2.2. Pristine membrane preparation

The pristine PVDF membrane was fabricated via an electrospinning machine (SS 20H, Ucalery, China). PVDF (10 wt.%) was firstly dissolved in binary solution of DMAc and acetone (4: 1 in weight) by stirring at 300 rpm and 50°C for 12 h. After standing for 12 hours to remove bubbles, 10 mL of the obtained homogeneous solution was loaded into a plastic syringe connected to a metal needle (with an inner diameter of 0.51 mm). The distance between the needle tip and the collector (covered with aluminum foil) was 16 cm, and the collector rotation speed was 50 r min^{-1}. The electrospinning solution was ejected at 0.065 mm min^{-1} under voltage difference of 14 kV (positive: +13 kV, negative: −1 kV). The temperature and relative humidity during electrospinning process were set to 25 ± 3°C and 45 ± 5%, respectively. After electrospinning, the electrospun membrane was heated at 60°C for 2 h to completely evaporate residual solvent before further treatment.

2.3. COF-LZU1 membrane modification

TFB (0.16, 0.32 and 0.48 g) and PDA (0.16, 0.32 and 0.48 g) were dissolved in 20 mL 1,4-dioxane in succession by stirring at 25°C for 10 min. The weight ratio of TFB: PDA in this COF-LZU1 precursor solution was 1:1. The as-prepared pristine

PVDF membrane was pre-immersed into the COF-LZU1 precursor solution for 30 min (as shown in Figure 1 (a)). Acetic acid (0.2, 0.4 and 0.6 mL) was added dropwise with stirring as trigger, and then the pre-immersed pristine PVDF membrane was re-immersed for 2 min. Later, the membrane was heated at 120°C for 12 h to induce the COF-LZU1 synthesis on electrospun PVDF fibers. Afterwards, the membrane was rinsed by 1,4-dioxane and ethanol for at least 3 times, respectively. The COF-LZU1 modified membrane was obtained after drying at 60°C for 2 h, and was denoted as COF-LZU1@PVDF-1, COF-LZU1@PVDF-2 and COF-LZU1@PVDF-3, respectively, according to the different amounts of TFB, PDA and acetic acid. In addition, the optimal COF-LZU1 modified membrane was selected according to their MD performance in the treatment for saline oil-in-water emulsion consisted of 3.5 wt.% NaCl and 2.0 g L^{-1} *n*-hexadecane.

2.4. Membrane characterization

The effects of COF-LZU1 modification on membrane characteristics (*e.g.*, structure, component and wettability) were investigated. The morphologies of pristine PVDF and COF-LZU1 modified membranes were compared by field-emission scanning electron microscopy (FESEM, Sirion 200, FEI, USA) from the top surface and cross section. The membrane surface roughness was evaluated by a confocal laser scanning microscope (CLSM, A 1, Nikon, Japan). The membrane pore size distribution was determined using bubble-point pressure method on a pore size analyzer (3H-2000PB, Beishide, China). The membrane porosity was calculated according to the weighing method as follows:

$$\varepsilon = \frac{m_w - m_d}{\rho A \delta} \quad (1)$$

where m_w is the mass of wet membrane after immersed in isopropanol solution for 24 h (g), m_d is the mass of dry membrane (g), ρ is the density of isopropanol (g cm^{-3}), A is the effective membrane area (m^2), and δ is the membrane thickness (m).

The functional groups on membrane surfaces were investigated by a Fourier transform infrared spectrometer in attenuated total reflectance mode (ATR-FTIR, Nicolet 6700, Thermo Scientific, USA) over the range of 3800–600 cm^{-1}. The element compositions of membrane surfaces were determined by X-ray photoelectron spectroscopy (XPS) using a Kratos Axis Ultra^{DLD} spectrometer (Shimadzu-Kratos, Japan). The membrane wettability was evaluated by liquid contact angles (DI water and *n*-hexadecane) via a goniometer (Dropmeter A-200, MAIST, China). Every measurement was conducted in triplicate for average.

2.5. DCMD performance test

The lab-scale direct contact membrane distillation (DCMD) system mainly consisted of membrane module, feed circulation with heating system and permeate circulation with condens-

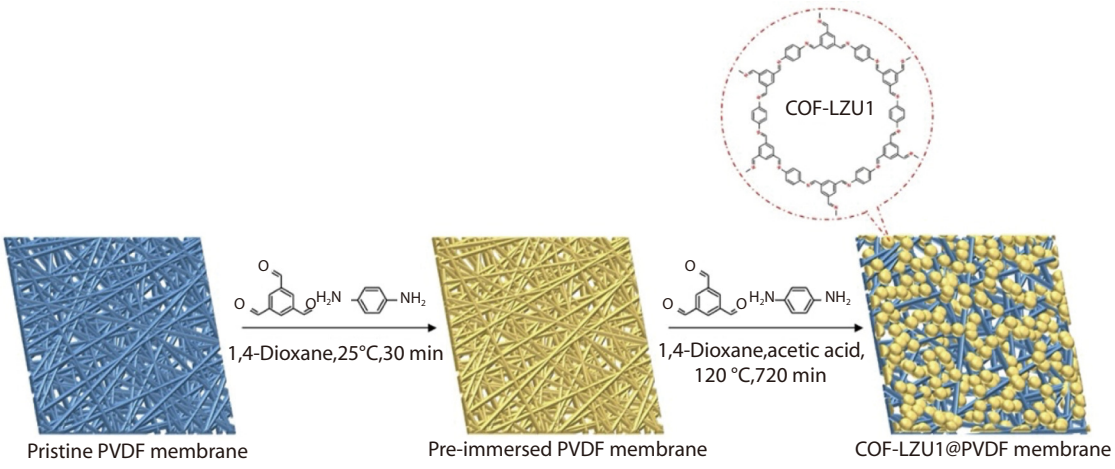

(a)

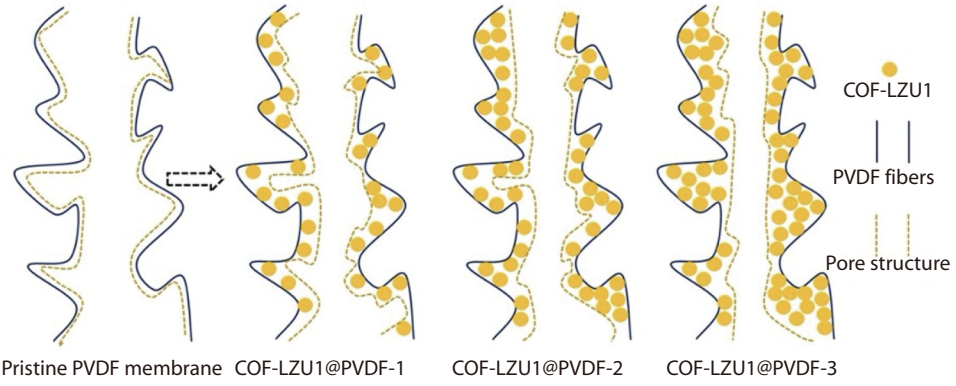

(b)

Fig. 1. Schematic illustrations of (a) membrane preparation and (b) membrane pore structure variations.

ing system. The effective area of installed membrane (including pristine PVDF, COF-LZU1@PVDF-1, COF-LZU1@PVDF-2 and COF-LZU1@PVDF-3 membranes) was 9.6 cm^2. DCMD desalination test was operated for 360 min using saline oil-in-water emulsion and DI water as the feed and permeate, respectively. The well-dispersed homogeneous emulsion was prepared by adding 2.0 g L^{-1} *n*-hexadecane into 3.5 wt.% NaCl solution, and then stirring at 2000 rpm for 1 h. The flow rates of feed (2.0 L) and permeate (0.5 L) were set at 1.0 and 0.5 L min^{-1}, respectively. The prepared emulsion could maintain stable during DCMD operation (6 h) without obvious precipitation due to the stirring and circulation. The corresponding temperatures of feed and permeate were controlled at 60 and 20 °C, respectively. To further investigate the membrane desalination performance, different saline oil-in-water emulsions with different *n*-hexadecane concentrations (0.0, 1.0, 2.0, 3.0 and 4.0 g L^{-1}) or temperatures (50, 60, 70 and 80°C) were used. The size distribution of the oil droplets in these prepared saline oil-in-water emulsions was determined by using a MAE-3000 from Malvern Instruments. The weight and conductivity variations in permeate were recorded every 15 min after 15 min pre-stabilization for desalination performance and membrane status evaluation.

The water flux (J, kg m^{-2} h^{-1}) was calculated according to Eq. (2):

$$J = \frac{\Delta m_p}{\rho A \Delta t} \tag{2}$$

where Δm_p is the increase of permeate weight (kg), ρ is the water density (kg m^{-3}) and Δt is the time interval (h).

The salt rejection rate (SR, %) was calculated according to Eq. (3):

$$SR(\%) = \left(1 - \frac{\Delta C_p}{C_f}\right) \times 100\% \tag{3}$$

where C_f is the initial feed conductivity (μs cm^{-1}) and ΔC_p is the increase of permeate conductivity (μs cm^{-1}).

2.6. Mechanism analysis

2.6.1. Anti-fouling

XDLVO analysis is usually used to quantify the interaction between membrane surface and hydrophobic oil compounds. The total free energy of interaction (ΔG^{XDLVO}) at the interface is a sum of Van der Waals energy component (ΔG^{LW}), Lewis acid-base energy component (ΔG^{AB}) and electrostatic double layer energy component (ΔG^{EL}). In our previous study, ΔG^{EL} was found to be negligible due to the nearly neutral Zeta potential of *n*-hexadecane (1.2 mV). Therefore, only ΔG^{LW} and ΔG^{AB} are considered in this study. The positive ΔG^{XDLVO} represents a repulsive force between hydrophobic oil compounds and membrane surface to mitigate membrane fouling, while a negative ΔG^{XDLVO} usually causes an attraction force that aggravates membrane fouling[23,24].

The calculations of interfacial free energy using surface tension components were as shown below:

$$\Delta G^{XDLVO} = \Delta G^{LW} + \Delta G^{AB} \tag{4}$$

$$\Delta G^{LW} = -2\left(\gamma_l^{LW} + \sqrt{\gamma_f^{LW}\gamma_m^{LW}} - \sqrt{\gamma_f^{LW}\gamma_l^{LW}} - \sqrt{\gamma_m^{LW}\gamma_l^{LW}}\right) \tag{5}$$

$$\Delta G^{AB} = 2\sqrt{\gamma_l^+}\left(\sqrt{\gamma_f^-} + \sqrt{\gamma_m^-} - \sqrt{\gamma_l^-}\right) + 2\sqrt{\gamma_l^-}\left(\sqrt{\gamma_f^+} + \sqrt{\gamma_m^+} - \sqrt{\gamma_l^+}\right) - 2\left(\sqrt{\gamma_f^+\gamma_m^-} + \sqrt{\gamma_f^-\gamma_m^+}\right) \tag{6}$$

where γ^{LW} is the surface tension parameter of LW energy component (mJ m^{-2}), γ^+ and γ^- are electron acceptor component and electron donor component of γ^{AB}, respectively, subscripts l, f and m represent liquid, foulant and membrane, respectively.

The surface tension parameters of membrane and foulant were calculated based on the contact angles of probe liquids (DI water, glycerol and diiodomethane) according to following equations. The calculated surface tension parameters for these three liquids were listed in Table S1. In addition, note that the determination of surface tension parameters based on the contact-angle measurement on porous and rough surfaces might be prone to errors, as the presented equations are initially derived for atomically smooth surfaces. Therefore, the calculations in XDLVO analysis are mainly used to reflect the tendency before and after modification rather than the detailed values.

$$(1 + \cos\theta)\,\gamma_l^{XDLVO} = 2\left(\sqrt{\gamma_s^{LW}\gamma_l^{LW}} + \sqrt{\gamma_s^+\gamma_l^-} + \sqrt{\gamma_l^+\gamma_s^-}\right) \tag{7}$$

$$\gamma^{AB} = 2\sqrt{\gamma^+\gamma^-} \tag{8}$$

$$\gamma^{XDLVO} = \gamma^{LW} + \gamma^{AB} \tag{9}$$

2.6.2. Anti-wetting

LEP is defined as the critical pressure at which liquid begins to penetrate across the membrane. LEP values of pristine PVDF and COF-LZU1 modified membranes for different saline oil-in-water emulsions were measured on a dead-end filtration. When the first liquid droplet across the membrane was observed, the used pressure value was recorded as LEP value.

In addition, LEP value also could be calculated by the following equation:

$$LEP = -\frac{2B\gamma\cos\theta}{r_{max}} \tag{10}$$

where B is the membrane pore shape factor (usually assigned as 0.4-0.85), γ is the surface tension of solution (N m^{-1}), θ is the contact angle on membrane surface (°), and r_{max} is the maximum membrane pore size (μm). During the LEP value measurement for COF-LZU1 modified membrane, the higher contact angle between pristine PVDF substrate and COF-LZU1 layer was regarded as the contact angle on COF-LZU1 modified membrane.

3. Results and Discussion

3.1. Membrane characterization

3.1.1. Membrane morphology and roughness

Figure 2 compares the top surface SEM micrographs of pristine PVDF membrane and COF-LZU1 modified membranes. It showed that the pristine PVDF membrane was symmetric and porous, constructed by randomly arranged electrospun PVDF fibers (Figure 2 (a)). During COF-LZU1 modification, two

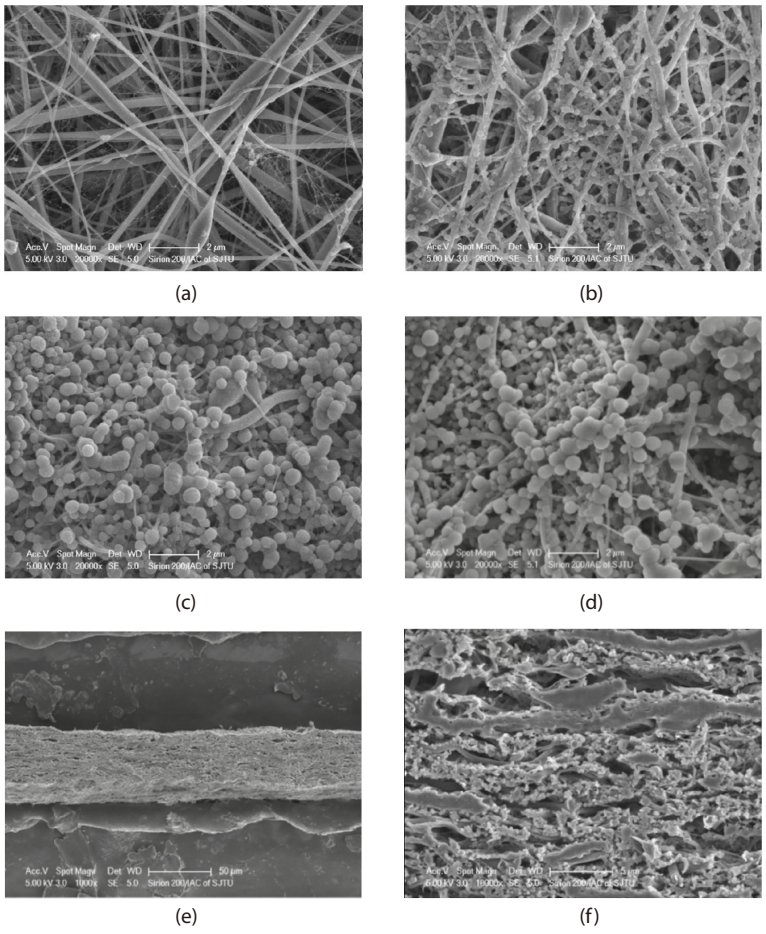

Fig. 2. SEM micrographs of the prepared membranes. Top surface of (a) pristine PVDF, (b) COF-LZU1@PVDF-1, (c) COF-LZU1@PVDF-2 and (d) COF-LZU1@PVDF-3 membranes. Cross section of COF-LZU1@PVDF-2 membrane with magnification of (e) 1000 and (f) 10000.

monomers TFB and PDA in solution uniformly dispersed among the electrospun PVDF fibers. After the addition of acetic acid, the in-situ synthesis of COF-LZU1 started via reversible covalent bond formation, and then the formed COF-LZU1 nanospheres uniformly distributed and condensed on the electrospun PVDF fibers. Meanwhile, the initial white membrane surface gradually became yellow with the attachment of numerous yellow COF-LZU1 nanospheres. As shown in Figure 2 (b), the mean diameter of formed COF-LZU1 nanospheres on COF-LZU1@PVDF-1 membrane was about 200.6 nm. With further increase of monomer concentrations, larger COF-LZU1 nanospheres with mean diameters of 375.5 nm and 385.8 nm were observed on COF-LZU1@PVDF-2 and COF-LZU1@PVDF-3 membranes, respectively (Figure 2 (c) and (d)). A positive correlation between the concentration of organic linker and the size of formed COF-LZU1 nanospheres was established. In addition, the fibrous surface of pristine PVDF membrane was gradually covered by the newly formed COF-LZU1 nanospheres in a layer-sheet arrangement, which generated a Janus-like membrane structure. The cross-section morphologies of COF-LZU1@PVDF-2 membrane in Figure 2 (e) and (f) showed that the COF-LZU1 nanospheres were uniformly distributed not only on the membrane surface but also in the substrate, which partially blocked the membrane pore and affected the pore structure.

Surface roughness characteristics of different membranes were calculated according to the CLSM images as shown in Figure S1. The red and blue colors are used to represent the convex area and concave area, respectively, meanwhile the deepening of color indicates the increase on concavity of membrane surface. Relatively even color distribution was exhibited on the smooth pristine PVDF membrane surface with S_a value of 0.84 μm. In comparison, complex and diversiform nanostructures presented after COF-LZU1 formation and significantly enhanced the surface roughness. Thereby, distinct differences on patterns of color distribution were exhibited on COF-LZU1 modified membranes. As the increase of TFB and PDA concentrations, growing S_a values of 1.17 μm, 1.22 μm and 1.22 μm were shown on COF-LZU1@PVDF-1, COF-LZU1@PVDF-2 and COF-LZU1@PVDF-3 membranes, respectively, which were 39.3%-45.2% higher than that of pristine PVDF membrane.

3.1.2. Membrane pore structure

Table 1 summarizes the membrane pore characteristics before and after COF-LZU1 modification. The pore size of pristine PVDF membrane was measured to be 0.80±0.34 μm. After modification, the pore sizes of COF-LZU1@PVDF-1, COF-LZU1@PVDF-2 and COF-LZU1@PVDF-3 membranes decreased to 0.69±0.25, 0.67±0.28 and 0.66±0.30 μm, respectively. These data confirmed that the in-situ synthesis of COF-LZU1 nanospheres would partially block the intrinsic membrane pores. As illustrated in Figure 1 (b), the initial interconnected pore structure with high tortuosity gradually changed to the straight pore structure with low tortuosity in some extent. During COF-LZU1 modification, acetic acid penetrated into the pores of electrospun PVDF substrate, inducing in-pore COF-LZU1 synthesis and a slight reduction in average pore size. How-

Table 1. Membrane pore characteristics comparison of different membranes.

Membrane	Pore size (μm)	Porosity (%)	Thickness (μm)
Pristine PVDF	0.80±0.34	85.5±1.7	58.0±3.5
COF-LZU1@PVDF-1	0.69±0.25	55.1±4.8	
COF-LZU1@PVDF-2	0.67±0.28	57.3±3.3	
COF-LZU1@PVDF-3	0.66±0.30	59.8±3.5	

ever, excessively high TFB/PDA concentrations caused COF-LZU1 aggregates to preferentially form in solution or on the membrane surface, compromising the pore structure re-construction ability. Thus, no further pore size reduction occurred in COF-LZU1@PVDF-2 and COF-LZU1@PVDF-3.

As another important factor in determining desalination performance of MD membrane[25,26], the pore size distributions of COF-LZU1@PVDF-1, COF-LZU1@PVDF-2 and COF-LZU1@PVDF-3 membranes were smaller than that of pristine PVDF membrane, which was usually considered to be beneficial for membrane wetting prevention[27]. The corresponding porosity analysis showed that the porosity of pristine PVDF membrane was 85.5±1.7%, and gradually decreased to 55-59% after COF-LZU1 modification: 55.1±4.8% for COF-LZU1@PVDF-1, 57.3±3.3% for COF-LZU1@PVDF-2 and 59.8±3.5% for COF-LZU1@PVDF-3 membranes, respectively.

3.1.3. Membrane chemical component

The surface chemistry variation before and after COF-LZU1 modification was investigated by ATR-FTIR and XPS. The obtained ATR-FTIR spectra of pristine PVDF membrane and COF-LZU1 modified membranes were presented in Figure 3 (a). It was observed that the pristine PVDF membrane exhibited typical peaks at 841 cm^{-1}, 1180 cm^{-1}, 1277 cm^{-1} and 1400 cm^{-1}, which were assigned to the asymmetric stretching of CF_2 group in the β or γ phase, symmetrical stretching of CF_2 group, the γ phase of PVDF, and CH_2 bending/scissoring vibrations, respectively[28-30]. After in-situ growth of COF-LZU1, characteristic peaks of the CH=O group (from TFB) and the N-H group (from PDA) appeared at 1695 cm^{-1} and 3100-3500 cm^{-1}, respectively[15,31]. Moreover, a peak at 1618 cm^{-1}, assigned to the C=N stretching vibration (produced by condensation reaction from TFB and PDA), was detected in the spectra of COF-LZU1@PVDF-1, COF-LZU1@PVDF-2 and COF-LZU1@PVDF-3 membranes. With the increase in the concentrations of two monomers, the intensity of the 1618 cm^{-1} peaks gradually increased, attributable to the higher density of C=N groups.

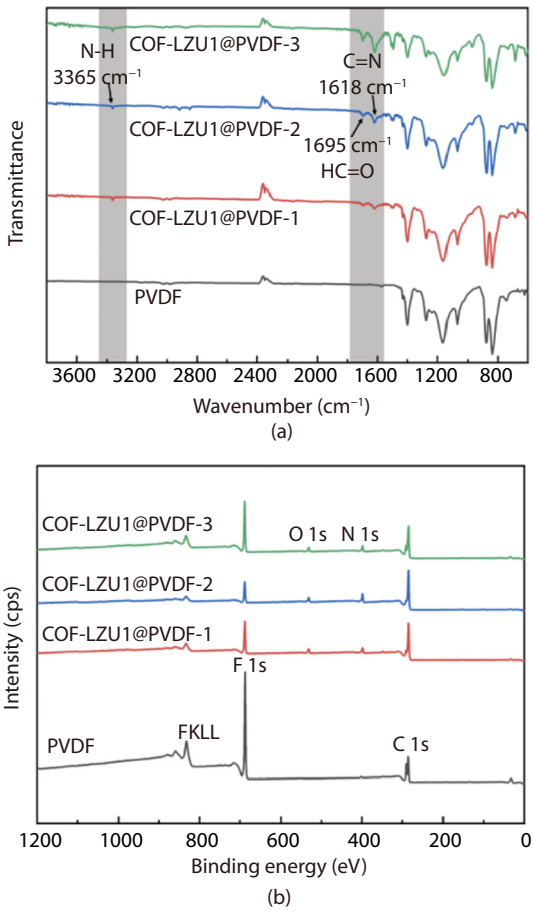

Fig. 3. (a) FTIR-ATR spectra and (b) XPS spectra of different membranes.

The elemental composition of different membranes was further analyzed by XPS spectra (Figure 3 (b)). For the pristine PVDF membrane, two main peaks were detected at 292 eV and 689 eV, corresponding to C and F elements, respectively, while element H was unmeasurable in XPS. The introduction of COF-LZU1 induced two additional elements: O (O1s peak at 533 eV) and N (N1s peak at 401 eV). Consequently, five main peaks were observed in the XPS spectra of the COF-LZU1 modified membranes, consistent with the FTIR data. Collectively, these observations clearly confirmed the successful synthesis of COF-LZU1 on the pristine PVDF membrane.

3.1.4. Membrane wettability

Contact angle measurements for DI water and oil-in-water emulsion (2.0 g L^{-1} *n*-hexadecane) were used to evaluate the wettability of COF-LZU1 layer, pristine PVDF membrane and COF-LZU1@PVDF-2 membrane. As shown in Figure S2 (a), the values of water contact angle and emulsion contact angle on COF-LZU1 layer were 79.9° and 133.7°, respectively. This hydrophilic COF-LZU1 layer was also oleophobic that could efficiently limit the deposition of *n*-hexadecane on membrane surface. In comparison, the water contact angle on pristine PVDF membrane was 140.5°, while the emulsion contact angle was 101.4° (Figure S2 (b)). After the corporation of COF-LZU1 layer and pristine PVDF substrate, the COF-LZU1@PVDF-2 membrane exhibited a water contact angle of 108.5° and an emulsion contact angle of 107.2° (Figure S2 (c)). These data showed that this COF-LZU1 modified membrane was more suitable to repel the *n*-hexadecane deposition in comparison with pristine PVDF substrate, while it still could prevent the direct invasion of oil-in-water emulsion.

3.2. DCMD performance for emulsion using different membranes

Figure 4 shows the water fluxes and permeate conductivities of different membranes in treating saline oil-in-water emulsion consisted of 3.5 wt.% NaCl and 2.0 g L^{-1} *n*-hexadecane. It is usually considered that relatively large membrane pore of

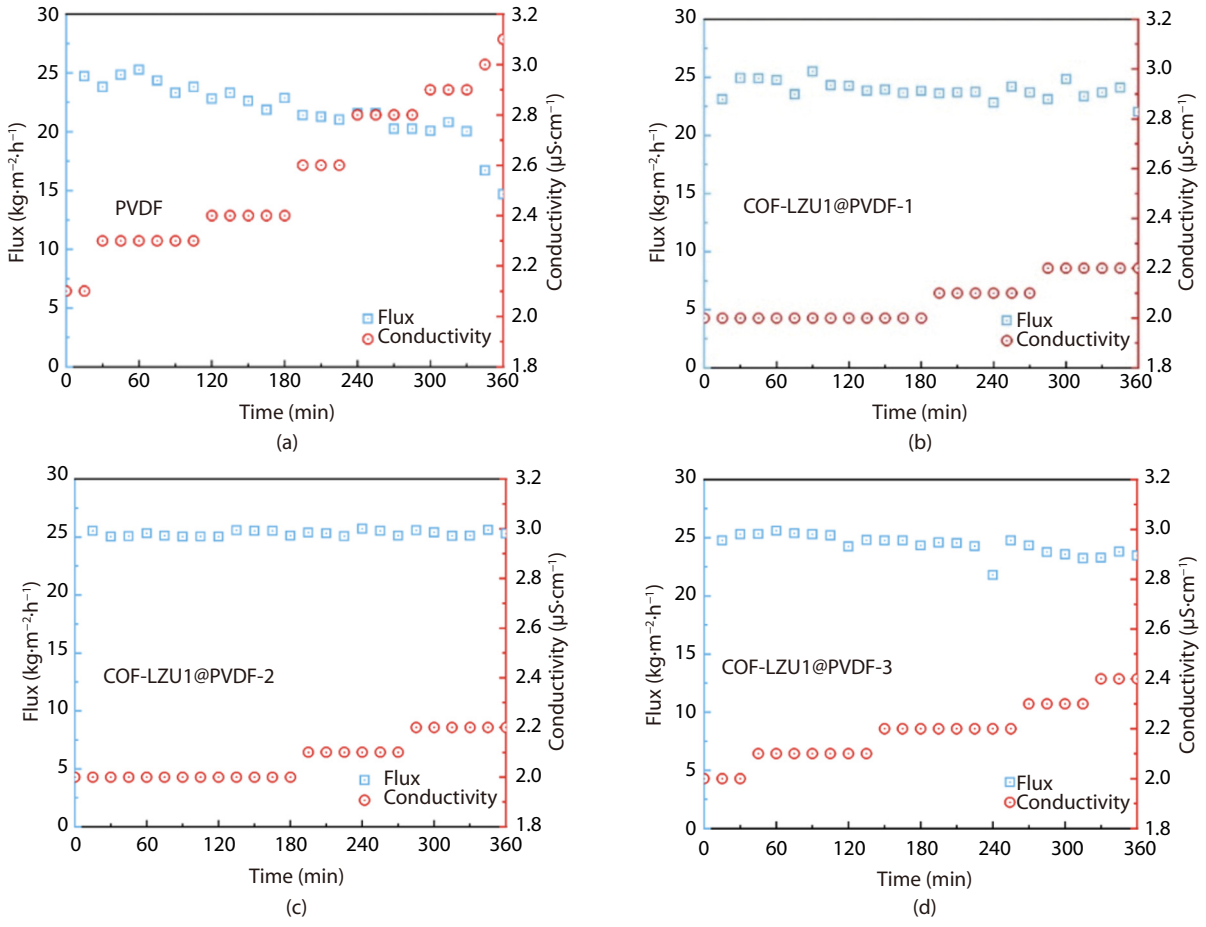

Fig. 4. Water flux and permeate conductivity variations in DCMD for saline oil-in-water emulsion using (a) pristine PVDF, (b) COF-LZU1@PVDF-1, (c) COF-LZU1@PVDF-2 and (d) COF-LZU1@PVDF-3 membranes.

pristine PVDF membrane should have facilitated the water vapor transmembrane transfer and resulted in high water flux[32]. However, the initial water flux of pristine PVDF membrane was 24.7 kg m^{-2} h^{-1}, while similar water fluxes were observed on COF-LZU1 modified membranes: 23.1, 25.5 and 24.8 kg m^{-2} h^{-1} for COF-LZU1@PVDF-1, COF-LZU1@PVDF-2 and COF-LZU1@PVDF-3 membranes, respectively. Although the mean pore size of pristine PVDF membrane was larger than other membranes, the reflection probabilities in the water vapor transport channels were higher than the COF modified membranes due to the higher membrane tortuosity[21,22]. As a result, the diffusion length of water vapor was prolonged, thus leading to the reduction on water permeation flux. In comparison, the water vapor transport channels of COF-LZU1 modified membranes became straighter, thus the water vapor reflection was alleviated and the water vapor diffusion length was shortened. Besides, the presence of hydrophilic COF-LZU1 layer partially reduced the hydrophobic PVDF substrate thickness to shorten the total water vapor transmembrane path. This hydrophilic COF layer was also beneficial in improving heat transfer from hot feed to feed-membrane interface as compared to the PVDF substrate, and thus inhibiting the effect of temperature polarization to maintain the transmembrane driving force[33]. Note that the average water flux during 360 min followed an order of COF-LZU1@PVDF-2 membrane (25.3±0.1 kg m^{-2} h^{-1}) > COF-LZU1@PVDF-3 membrane (24.4±0.8 kg m^{-2} h^{-1}) > COF-LZU1@PVDF-1 membrane (23.9±0.6 kg m^{-2} h^{-1}), which was mainly attributable to the synergistic effect of re-constructed pore structure and added hydrophilic layer.

Afterwards, it should be noted that the pristine PVDF membrane experienced obvious water flux decline (41.3%) in 360 min. The water flux slightly declined from 75 min to 330 min, then rapidly decreased to 14.5 kg m^{-2} h^{-1} at the end. The corresponding permeate conductivity increase was only 1.1 μS cm^{-1} without obvious fluctuation, which implied that the membrane fouling occurred due to the hydrophobic-hydrophobic interaction between membrane surface and *n*-hexadecane. In comparison, no obvious water flux decline or conductivity variation was detected on the COF-LZU1 modified membranes. It is usually considered that the hydrophilic COF-LZU1 layer induced the hydration shell formation to provide high repellence for *n*-hexadecane and prevent its adhesion on membrane surface[34,35]. Thereby, the membrane fouling propensity on COF-LZU1 modified membranes was mitigated, and the COF-LZU1@PVDF-2 membrane was used for the further investigation due to its highest water flux.

3.3. Effect of emulsion parameter on DCMD performance

3.3.1. Concentration

Figure 5 depicts the DCMD desalination performance of pristine PVDF membrane and COF-LZU1@PVDF-2 membrane in treating saline oil-in-water emulsion with different concentrations of *n*-hexadecane. Composition of feed greatly influences the membrane fouling and wetting propensities mainly via the pollutant property and the interfacial interaction between

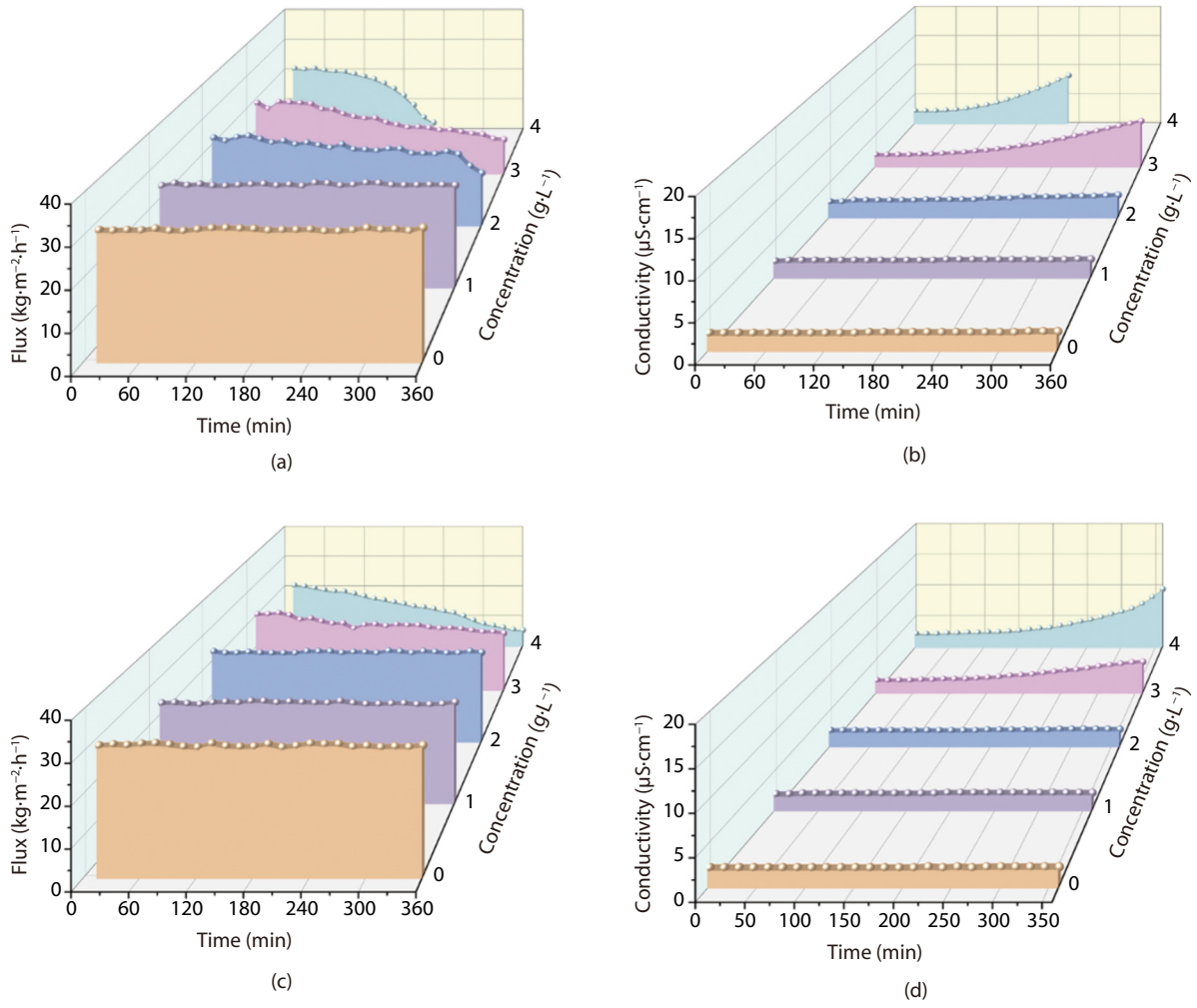

Fig. 5. Water flux and permeate conductivity variations in DCMD using (a, b) pristine PVDF and (c, d) COF-LZU1@PVDF-2 membranes for saline oil-in-water emulsions containing 1, 2, 3 and 4 g L^{-1} *n*-hexadecane.

membrane surface and pollutant[36]. The non-fouled/wetted status of common hydrophobic electrospun membrane is easily to maintain when treating 3.5 wt.% NaCl solution with high surface tension (⩾ 72.8 mN m^{-1}). As shown in Figure 5 (a) and (b), the pristine PVDF membrane exhibited stable desalination performance with an average water flux of 30.8 kg m^{-2} h^{-1} during 360 min DCMD without permeate conductivity increase. The presence of *n*-hexadecane not only decreased the feed surface tension but also induced the adhesion on membrane surface. The membrane fouling induced pore blocking would lead to the compromise on water flux without affecting the permeate quality[37]. The droplet size distribution analysis showed that the mean diameter of oil droplet gradually increased to 485.4-900.8 μm with the increase of *n*-hexadecane concentration from 1.0 to 4.0 g L^{-1}, respectively. Thus, the initial water flux of pristine PVDF membrane decreased to 26.1 kg m^{-2} h^{-1} in treating saline oil-in-water emulsion with 1.0 g L^{-1} *n*-hexadecane. The further increase on *n*-hexadecane concentration greatly increased the risks of membrane fouling even membrane wetting, resulting in the pristine PVDF membrane experienced severe water flux decline and conductivity increase from the onset of DCMD test. When the *n*-hexadecane concentration increased to 4.0 g L^{-1}, the initial water flux was only 20.1 kg m^{-2} h^{-1} and then dramatically dropped to almost zero with dramatically increased conductivity variation of 6.1 μS cm^{-1} within 225 min, suggesting that the pristine PVDF membrane was completely wetted[38].

For the COF-LZU1@PVDF-2 membrane, its hydrophilic COF-LZU1 layer was oleophobic underwater, which could effectively deter the adhesion of *n*-hexadecane on membrane surface and alleviate the blockage of membrane pore. Compared with the large membrane pore of pristine PVDF membrane that was prone to membrane wetting, the narrowed pores of COF-LZU1 modified membranes were also more suitable to prevent the feed penetration, thus avoiding the reduction on water flux and the deterioration on permeate quality[21,39]. Therefore, the compromise on desalination performance was prevented especially at low *n*-hexadecane concentrations. As shown in Figure 5 (c) and (d), no obvious water flux decline or conductivity increase was observed in the treatment of saline oil-in-water emulsion containing 1.0 and 2.0 g L^{-1} *n*-hexadecane. Facing the most concentrated emulsion with 4.0 g L^{-1} *n*-hexadecane, the initial water flux of COF-LZU1@PVDF-2 membrane still was 20.3 kg m^{-2} h^{-1} and maintained at 4.5 kg m^{-2} h^{-1} after 360 min. Meanwhile, the conductivity variation was 7.3 μS cm^{-1} (salt rejection rate>99.9%), suggesting the membrane wetting had been alleviated in comparison with the pristine PVDF membrane.

3.3.2. Temperature

Figure 6 compares the DCMD desalination performance of pristine PVDF membrane and COF-LZU1@PVDF-2 membrane in

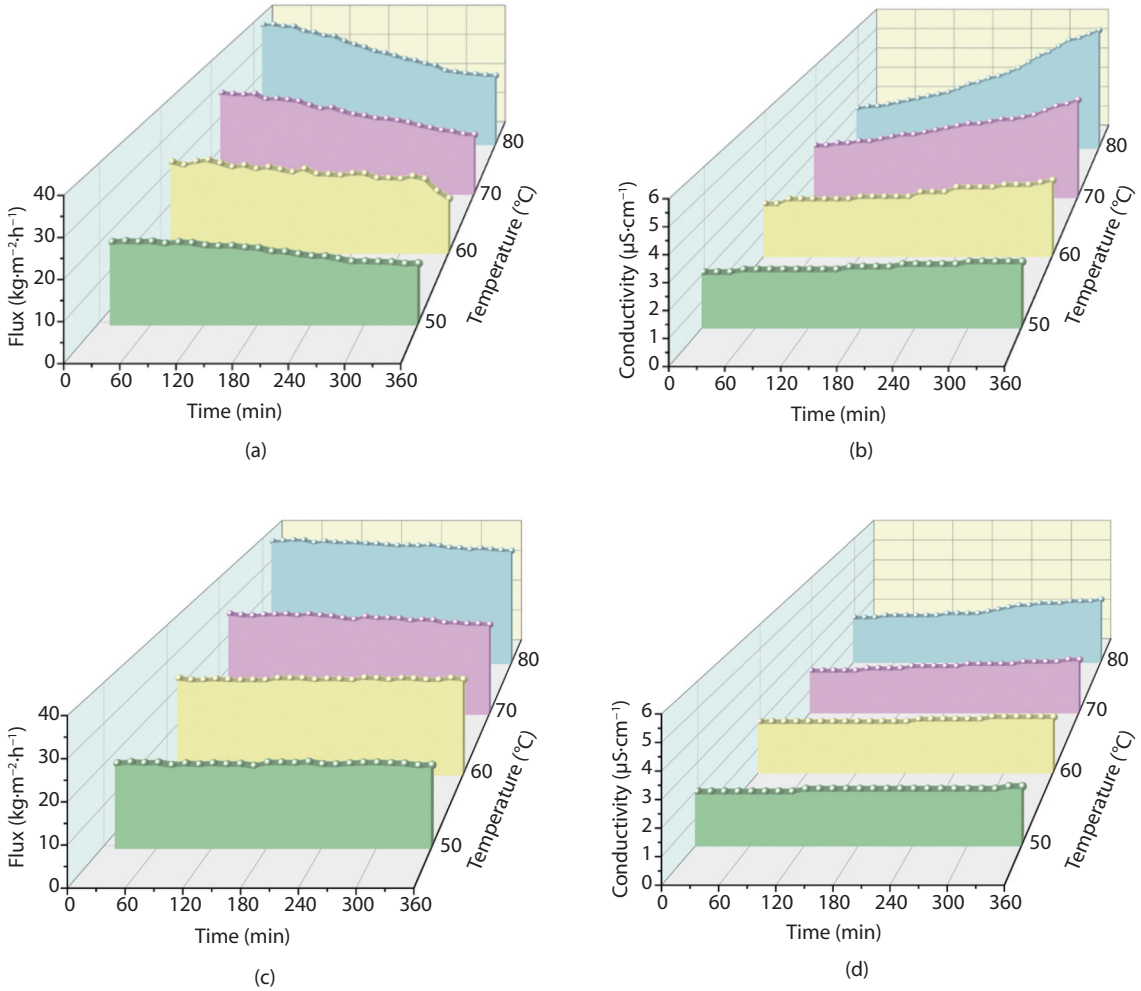

Fig. 6. Water flux and permeate conductivity variations in DCMD using (a, b) pristine PVDF and (c, d) COF-LZU1@PVDF-2 membranes for saline oil-in-water emulsions at 50, 60, 70 and 80°C.

treating saline oil-in-water emulsion at different temperatures. The feed temperature is one of the main parameters in DCMD that determines the water vapor transmembrane transport[40]. In general, the transmembrane vapor pressure exponentially increases with feed temperature, thereby significantly enhancing water flux. As shown in Figure 6 (a) and (b), the initial water flux of pristine PVDF membrane was 20.1 kg m^{-2} h^{-1} at feed temperature of 50°C. When the temperature of feed was adjusted to 60, 70 and 80°C, the initial water flux increased to 24.7, 30.2 and 39.1 kg m^{-2} h^{-1} due to the gradually increased transmembrane temperature difference and corresponding driving force. However, the LEP values of membrane were reduced with the increasing feed temperature due to the reduced shape factor of membrane pore (B) and surface tension of feed (γ), which was prone to membrane wetting[41]. As a result, the accelerated membrane wetting phenomenon was observed, and the decline range and rate of water flux were positively correlated with the feed temperature. Finally, the water flux decreased 42.6% to 22.4 kg m^{-2} h^{-1} at 80°C feed temperature after 360 min. These data stated that the membrane wetting on pristine PVDF membrane became more and more severe with the increase on feed temperatures, which was consistent with other literature[42]. In comparison, the COF-LZU1@PVDF-2 membrane with hydrophilic COF-LZU1 layer exhibited less tendency towards membrane wetting even at higher feed temperatures. This COF-LZU1 layer also could alleviate the temperature polarization to maintain relatively high transmembrane driving force[33]. Therefore, only partial wetting was observed on the COF-LZU1 modified membrane during the treatment for saline oil-in-water emulsion with slight compromise on water flux or permeate quality (as shown in Figure 6 (c) and (d)).

3.4. Mechanism analysis

3.4.1. Anti-fouling

XDLVO analysis was used to explain membrane fouling propensity via the interactions between *n*-hexadecane and membrane surface. As shown in Table S2, the surface tension component parameters of γ^+, γ^-, γ^{LW}, γ^{AB} and γ^{TOT} were calculated according to the measured contacts angles of probe liquids on pristine PVDF and COF-LZU1@PVDF-2 membranes. As an electron-donor component, γ^- reflects the affinity between membrane surface and water molecules[43]. The calculated γ^- value of COF-LZU1@PVDF-2 membrane were 0.54, significantly higher than that of pristine PVDF membrane (0.02). Undoubtedly, the COF-LZU1@PVDF-2 membrane with hydrophilic layer exhibited stronger affinity to water molecules and were more prone to forming hydration shell via hydrogen bonds with membrane surface. Although these determined surface tension parameters based on contact-angle on pristine and COF-LZU1 modified membrane surfaces might be prone to errors, the observed variation tendency could be used to reflect the

effect of COF-LZU1 modification.

According to these data, the interaction free energies of ΔG^{AB}, ΔG^{LW} and ΔG^{XDLVO} were further calculated. With the much higher absolute values than LW interaction energy, polar AB interaction energy played a more important role in determining the interaction between *n*-hexadecane and two membranes. The total interaction free energies (ΔG^{XDLVO}) of pristine PVDF and COF-LZU1@PVDF-2 membranes were −103.23 mJ m^{-2} and −88.58 mJ m^{-2}, respectively. The lower absolute value indicated that COF-LZU1@PVDF-2 membrane had lower attractive force for *n*-hexadecane, which led to weaker *n*-hexadecane adhesion and lower membrane fouling propensity.

3.4.2. Anti-wetting

It is widely assumed that membrane wetting occurs when the transmembrane pressure exceeds the LEP, and the higher LEP value, the higher wetting resistance[44]. Figure 7 summarizes the calculated LEP values of pristine PVDF and COF-LZU1@PVDF-2 membranes for saline oil-in-water emulsions with different *n*-hexadecane concentrations. As the increase on *n*-hexadecane concentration, the solution surface tension and membrane contact angle gradually decreased, thus the LEP values also gradually decreased. The LEP values of pristine PVDF membrane were calculated to be 61.5, 21.9 and 7.5 kPa at 1.0, 2.0 and 3.0 g L^{-1} *n*-hexadecane, respectively. It should be noted that the contact angle on pristine PVDF membrane was less than 90° when *n*-hexadecane concentrations was 4.0 g L^{-1}, resulting in a negative LEP value of -14.7 kPa. Therefore, LEP calculation is not applicable for hydrophilic membrane, and the critical LEP value was regarded as 0 kPa. Compared with pristine PVDF membrane, the re-constructed pore structure of COF-LZU1@PVDF-2 membrane was beneficial to obtain higher LEP. The calculated LEP values were 67.6, 39.1, 31.4 and 13.2 kPa, respectively, which were 9.9-315.8% higher than those of pristine PVDF membrane. To verify the accuracy of LEP calculation, the LEP values of two membranes for different saline oil-in-water emulsions were also measured and listed in Table S3. The measured LEP values of pristine PVDF membrane were 67.3 (1.0 g L^{-1}), 25.7 (2.0 g L^{-1}), 9.7 (3.0 g L^{-1}) and 1.3 kPa (4.0 g L^{-1} *n*-hexadecane) for different saline oil-in-water emulsions, while these data were 75.7, 42.3, 36.7 and 22.7 kPa on COF-LZU1@PVDF-2 membrane, respectively. These calculated and measured LEP values co-confirmed that COF-LZU1@PVDF-2 membrane could effectively resist the membrane wetting caused by saline oil-in-water emulsion even at higher concentration of *n*-hexadecane.

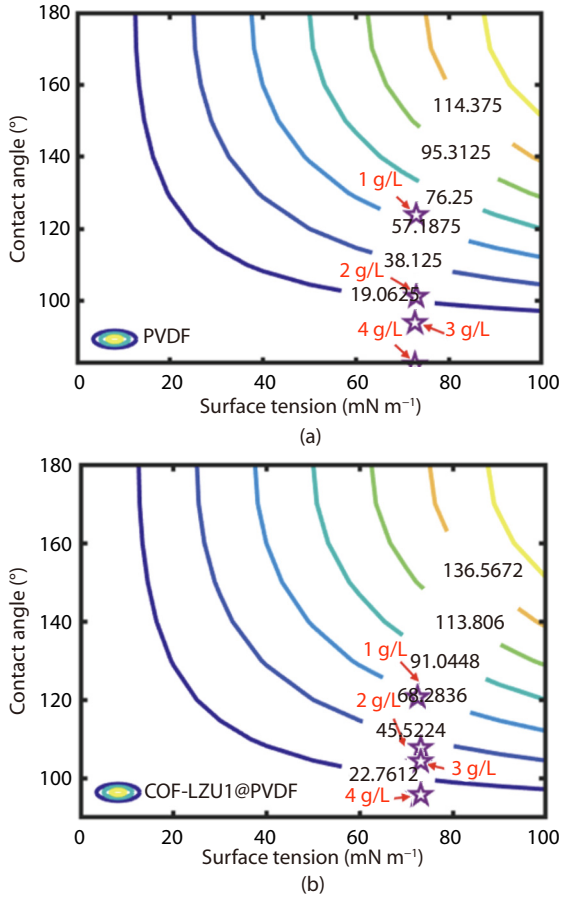

Fig. 7. Calculated LEP values for (a) pristine PVDF and (b) COF-LZU1@PVDF-2 membranes when treating saline oil-in-water emulsions with different *n*-hexadecane concentrations.

4. Conclusion

In this study, a novel Janus-like COF modified membrane (COF-LZU1@PVDF-2) was developed for MD for the first time via in-situ synthesis of COF-LZU1 on electrospun PVDF substrate. Membrane fouling and wetting, induced by *n*-hexadecane adhesion, were significantly alleviated, attributed to the synergistic effects of hydrophilic COF-LZU1 layer (with hydration shell) and the re-construction of pore structure into straight channel. An average water flux of 25.3 kg m^{-2} h^{-1} without compromising salt rejection was observed for the COF-LZU1@PVDF-2 membrane during treatment of saline oil-in-water emulsion (containing 3.5 wt.% NaCl and 2.0 g L^{-1} *n*-hexadecane) at 60°C. Further DCMD tests demonstrated that robust desalination performance, characterized by high water flux and excellent permeate quality, could be achieved under varying feed conditions (*n*-hexadecane concentrations and temperatures). The total interaction free energy and LEP value before and after COF-LZU1 modification were further calculated to clarify the underlying anti-fouling and anti-wetting mechanisms. This study provides insights into the design of COF-modified MD membranes for efficient treatment of saline oil-in-water emulsions.

Acknowledgements

This work is financially supported by Hainan Provincial Natural Science Foundation of China (No. 425QN398), Yunnan Fundamental Research Projects (No. 202501AT070053), Natural Science Foundation of Shanghai (No. 24ZR1435800), and Natural Science Foundation of Chongqing (No. CSTB2025NSCQ-GPX0469).

Conflict of Interest

The authors declare no conflict of interest.

Electronic Supplementary Material (ESM)

The online version contains supplementary material available at https://doi.org/10.26599/ECS.2025.9600005.

References

[1] Tian X, Song Y, Shen Z, et al. A comprehensive review on toxic petrochemical wastewater pretreatment and advanced treat-

ment[J]. *Journal of Cleaner Production*, 2020, 245: 118692.
[2] Hu J, Fu W, Ni F, et al. An integrated process for the advanced treatment of hypersaline petrochemical wastewater: A pilot study[J]. *Water Research*, 2020, 182: 116019.
[3] Huang Y, Luo M, Xu Z, et al. Catalytic ozonation of organic contaminants in petrochemical wastewater with iron-nickel foam as catalyst[J]. *Separation and Purification Technology*, 2019, 211: 269–278.
[4] Lu K J, Chen Y, Chung T-S. Design of omniphobic interfaces for membrane distillation – A review[J]. *Water Research*, 2019, 162: 64–77.
[5] Zhao S, Tao Z, Han M, et al. Hierarchical Janus membrane with superior fouling and wetting resistance for efficient water recovery from challenging wastewater via membrane distillation[J]. *Journal of Membrane Science*, 2021, 618: 118676.
[6] Park S H, Kim J H, Moon S J, et al. Enhanced, hydrophobic, fluorine-containing, thermally rearranged (TR) nanofiber membranes for desalination via membrane distillation[J]. *Journal of Membrane Science*, 2018, 550: 545–553.
[7] Li C, Deng W, Gao C, et al. Membrane distillation coupled with a novel two-stage pretreatment process for petrochemical wastewater treatment and reuse[J]. *Separation and Purification Technology*, 2019, 224: 23–32.
[8] Alkhudhiri A, Darwish N, Hilal N. Membrane distillation: A comprehensive review[J]. *Desalination*, 2012, 287: 2–18.
[9] Drioli E, Ali A, Macedonio F. Membrane distillation: Recent developments and perspectives[J]. *Desalination*, 2015, 356: 56–84.
[10] Zuo G, Wang R. Novel membrane surface modification to enhance anti-oil fouling property for membrane distillation application[J]. *Journal of Membrane Science*, 2013, 447: 26–35.
[11] Asad A, Rastgar M, Sameoto D, et al. Gravity assisted super high flux microfiltration polyamide-imide membranes for oil/water emulsion separation[J]. *Journal of Membrane Science*, 2021, 621: 119019.
[12] Wei X, Zhao B, Li X-M, et al. CF4 plasma surface modification of asymmetric hydrophilic polyethersulfone membranes for direct contact membrane distillation[J]. Journal of Membrane Science, 2012, 407-408: 164-175.
[13] Zhu Z, Liu Z, Zhong L, et al. Breathable and asymmetrically superwettable Janus membrane with robust oil-fouling resistance for durable membrane distillation[J]. *Journal of Membrane Science*, 2018, 563: 602–609.
[14] Rana D, Matsuura T. Surface Modifications for Antifouling Membranes[J]. *Chemical Reviews*, 2010, 110(4): 2448–2471.
[15] Fan H, Gu J, Meng H, et al. High-flux membranes based on the covalent organic framework COF-LZU1 for selective dye separation by nanofiltration[J]. *Angewandte Chemie International Edition*, 2018, 57(15): 4083–4087.
[16] Yang H, Cheng X, Cheng X, et al. Highly water-selective membranes based on hollow covalent organic frameworks with fast transport pathways[J]. *Journal of Membrane Science*, 2018, 565: 331–341.
[17] Huang J, Han X, Yang S, et al. Microporous 3D covalent organic frameworks for liquid chromatographic separation of xylene isomers and ethylbenzene[J]. *Journal of the American Chemical Society*, 2019, 141(22): 8996–9003.
[18] Fan H, Mundstock A, Feldhoff A, et al. Covalent organic framework–covalent organic framework bilayer membranes for highly selective gas separation[J]. *Journal of the American Chemical Society*, 2018, 140(32): 10094–10098.
[19] Ying Y, Peh S B, Yang H, et al. Ultrathin covalent organic framework membranes via a multi-interfacial engineering strategy for gas separation[J]. Advanced Materials, 2021: 2104946.
[20] Wang C, Li Z, Chen J, et al. Covalent organic framework modified polyamide nanofiltration membrane with enhanced performance for desalination[J]. *Journal of Membrane Science*, 2017, 523: 273–281.
[21] Zhao S, Jiang C, Fan J, et al. Hydrophilicity gradient in covalent organic frameworks for membrane distillation[J]. *Nature Materials*, 2021, 20(11): 1551–1558.
[22] Li Y, Chen H, Xiao S, et al. Ultrafast diameter-dependent water evaporation from nanopores[J]. *ACS Nano*, 2019, 13(3): 3363–3372.
[23] Bower M, Bank T L, Giese R F, et al. Nanoscale forces of interaction between glass in aqueous and non-aqueous media: A theoretical and empirical study[J]. *Colloids & Surfaces A Physicochemical & Engineering Aspects*, 2010, 362(1-3): 90–96.
[24] Feng L, Li X, Du G, et al. Adsorption and fouling characterization of Klebsiella oxytoca to microfiltration membranes[J]. *Process Biochemistry*, 2009, 44(11): 1289–1292.
[25] Woods J, Pellegrino J, Burch J. Generalized guidance for considering pore-size distribution in membrane distillation[J]. *Journal of Membrane Science*, 2011, 368(1): 124–133.
[26] Kim A S. A two-interface transport model with pore-size distribution for predicting the performance of direct contact membrane distillation (DCMD)[J]. *Journal of Membrane Science*, 2013, 428: 410–424.
[27] Liao Y, Wang R, Tian M, et al. Fabrication of polyvinylidene fluoride (PVDF) nanofiber membranes by electro-spinning for direct contact membrane distillation[J]. Journal of Membrane Science, 2013, 425-426: 30-39.
[28] Qing W , Shi, X, Deng Y, et al. Robust superhydrophobic-superoleophilic polytetrafluoroethylene nanofibrous membrane for oil/water separation[J]. *Journal of Membrane Science*, 2017, 540: 354–361.
[29] Xing C, Guan J, Li Y, et al. Effect of a room-temperature ionic liquid on the structure and properties of electrospun poly (vinylidene fluoride) nanofibers[J]. *Acs Applied Materials & Interfaces*, 2014, 6(6): 4447–57.
[30] Chiao Y-H, Cao Y, Ang M B M Y, et al. Application of superomniphobic electrospun membrane for treatment of real produced water through membrane distillation[J]. *Desalination*, 2022, 528: 115602.
[31] Xia Z, Zhao Y, Darling S B. Covalent organic frameworks for water treatment[J]. *Advanced Materials Interfaces*, 2021, 8(1): 2001507.
[32] Barbe A M, Hogan P A, Johnson R A. Surface morphology changes during initial usage of hydrophobic, microporous polypropylene membranes[J]. *Journal of Membrane Science*, 2000, 172(1): 149–156.
[33] Afsari M, Shon H K, Tijing L D. Janus membranes for membrane distillation: Recent advances and challenges[J]. *Advances in Colloid and Interface Science*, 2021, 289: 102362.
[34] Chen Y, Lu K J, Chung T-S. An omniphobic slippery membrane with simultaneous anti-wetting and anti-scaling properties for robust membrane distillation[J]. *Journal of Membrane Science*, 2020, 595: 117572.
[35] Chew N G P, Zhao S, Wang R. Recent advances in membrane development for treating surfactant- and oil-containing feed streams via membrane distillation[J]. *Advances in Colloid and Interface Science*, 2019, 273: 102022.
[36] Chang H, Liu B, Zhang Z, et al. A critical review of membrane wettability in membrane distillation from the perspective of interfacial interactions[J]. *Environmental Science & Technology*, 2021, 55(3): 1395–1418.
[37] Deka B J, Guo J, Khanzada N K, et al. Omniphobic re-entrant PVDF membrane with ZnO nanoparticles composite for desalination of low surface tension oily seawater[J]. *Water Research*, 2019, 165: 114982.
[38] Rezaei M, Warsinger D M, Lienhard V J H, et al. Wetting phenomena in membrane distillation: Mechanisms, reversal, and preven-

tion[J]. *Water Research*, 2018, 139: 329–352.

[39] Fan J, Wu H, Wang F. Evaporation-driven liquid flow through nanochannels[J]. *Physics of Fluids*, 2020, 32(1): 012001.

[40] Chen Y, Lu K-J, Liang C Z, et al. Mechanically strong Janus tri-bore hollow fiber membranes with asymmetric pores for anti-wetting and anti-fouling membrane distillation[J]. *Chemical Engineering Journal*, 2022, 429: 132455.

[41] Saffarini R B, Mansoor B, Thomas R, et al. Effect of temperature-dependent microstructure evolution on pore wetting in PTFE membranes under membrane distillation conditions[J]. *Journal of Membrane Science*, 2013, 429: 282–294.

[42] Ge J, Peng Y, Li Z, et al. Membrane fouling and wetting in a DCMD process for RO brine concentration[J]. *Desalination*, 2014, 344: 97–107.

[43] Bai Z, Zhang R, Wang S, et al. Membrane fouling behaviors of ceramic hollow fiber microfiltration (MF) membranes by typical organic matters[J]. *Separation and Purification Technology*, 2021, 274: 118951.

[44] Horseman T, Yin Y, Christie K S S, et al. Wetting, scaling, and fouling in membrane distillation: State-of-the-art insights on fundamental mechanisms and mitigation strategies[J]. *ACS ES&T Engineering*, 2021, 1(1): 117–140.